Supporting Information

Hersch et al. 10.1073/pnas.1320355111

SI Materials and Methods

Plant Material. All mutants were generated in the Col background. The *pif4pif5*, *hfr1*, *hfr1pif4pif5*, and *sav3-2/taa1* mutants have been described previously (1–3). The *hfr1taa1* and *pif4pif5taa1* mutants were obtained by crossing *sav3-2*, respectively, to *hfr1-101* and *pif4-101pif5* (*pil6-1*), and genotyping was performed as previously described (1–3). For *sav3-2*, genomic DNA was amplified with CF505 (AACATCCCCATGTCCGATTT) and CF506 (AACACAAGTTCGTCATGTCGC). After digestion with *Mnl1*, the WT fragment produces two bands of 220 and 108 bp, whereas the *sav3-2* is not digested.

Pharmacological Treatment. For picloram (Sigma-Aldrich)/α-(phenyl ethyl-2-one)-IAA (PEO-IAA) (provided by Ken-ichiro Hayashi, Okayama University of Science, Okayama, Japan)/L-kynurenine (Sigma-Aldrich)/yucasin (provided by T. Koshiba, Tokyo Metropolitan University, Tokyo, Japan) treatment, seedlings were first grown on 1/2 Murashige and Skoog (MS). After 4 d, the meshes were transferred onto new 1/2 MS plates containing different concentrations of the drugs or DMSO as a control. All products were kept frozen as a 1,000× concentrated stock in DMSO. Hypocotyl elongation during the treatment was measured as the difference of hypocotyl length between day 4 and day 8 and expressed relative to the elongation of seedlings grown on DMSO.

RNA Extraction and Quantitative RT-PCR. These experiments were performed as described in ref. 4. For real-time RT-PCR on dissected hypocotyls and cotyledons, 7-d-old seedlings grown on horizontal plates were harvested in cold acetone and vacuum infiltrated for fixation. Seedlings were moved to 70% (vol/vol) ethanol to dissect cotyledons and hypocotyls. After removal of ethanol, samples were ground with glass beads, and RNA was extracted using the RNeasy plant mini kit with on-column DNA digestion (Qiagen). RNA (200 ng) was used for the reverse transcription as described in ref. 5. Except when indicating in the figure legends, *YLS8* and *UBC10* were used as housekeeping genes.

Determination of Auxin Content. Aerial parts of seedlings were pooled, weighed, and frozen in liquid nitrogen for quantification of free IAA content. The sample fresh weight was around 10 mg, and five replicates were analyzed for each line and treatment. $^{13}C_6$-IAA (500 pg) internal standard was added to each sample, and the samples were purified and analyzed using gas chromatography coupled to tandem MS as described in ref. 6, with minor modifications.

Computational Methods. ***Model.*** The regulatory network was modeled using ordinary differential equations. The same general purpose equation was used to model molecular activity. It is given by

$$\dot{x}_i = s_i + \Sigma_j a_{ji} x_i - k_i x_i - \Sigma_j d_{ji} x_j x_i. \quad \textbf{[S1]}$$

Here x_i represents the activity of node i, in our case the molecular activity, and a_{ji} and d_{ji} are the weight of the positive and negative edges from node j to node i and are strictly positive. The positive source term s_i models all activating effects not explicitly represented in the network, such as baseline protein production. The degradation term $k_i x_i$ models all inactivating effects not explicitly in the network. In this equation, all effects are very coarsely approximated by a linear function, and the degradation term is bilinear. In sum, each positive edge corresponds to a linear activation, and each negative edge corresponds to a bilinear inhibition that ensures a positive activity. Relevant biological knowledge is also inserted in the model. For example, for mutants, the corresponding node activities are constrained to zero, and the ratio of phytochrome B (phyB) activity in high vs. low red light(R): far red light (FR) was set to 10, as documented by spectral measurements (7). Using contraction analysis (8), the system can be shown to converge to a single attractor as long as there is no cycle of positive edges in the network. The system is thus safely assumed to be at steady state. This set of equations differs from other general purpose network equations proposed in the literature, such as the Boolean network, continuous Boolean networks (5), or Hopfield-like networks (9). In those networks, activities have a lower and upper bound (usually zero and one). Our network only has a lower bound but no upper bound. This property, along with the use of linear activation terms, reduces the nonlinearity of the network, which is very advantageous for the performance of the sampling algorithm we subsequently use. It can be justified on a theoretically level by assuming that molecular activities do not reach saturation level. Indeed, there can be differences of many orders of magnitude in the concentrations of proteins and assigning a gating function to the activities is also somewhat arbitrary, especially as units are left unspecified. Only for the readout node, hypocotyl elongation, do we add a bounding sigmoidal function, because we know that the observed elongations belong to the same order of magnitude. The sigmoidal function takes the following form

$$y = \beta[1 + \exp(-x + \beta/2)]^{-1},$$

where β gives the amplitude (or saturation level) of the function, which has $\beta/2$ as a fixed point.

We define the network parameter vector θ consisting of the weight of all edges, the source and degradation terms of all nodes and β. Moreover, we set the list of experimental conditions λ as the (discrete) inputs of the network specifying the combinations of light conditions and the mutant used. We can then define the output vector $g(\theta, \lambda)$ as the values of the elongation at steady state when using parameter values θ and all experimental conditions λ. Therefore, for each parameter vector θ, there is a vector of outcomes $g(\theta, \lambda)$, specifying the values of the read-out node at steady state for each experimental condition in λ. These steady states are computed numerically.

The advantage of this model lies in its simplicity, as it only contains one effective parameter per node (s_i/k_i) and one parameter per edge. In the present study, the network topology is also kept as simple as possible. If needed, however, the role of additional players can be explored because both node and edges can be expanded into more detailed subnetworks as long as we can generate enough data to constrain it with the relevant mutant combinations.

As mentioned above, this model cannot model sensitivity because activations are linear. When needed, we modeled the influence of node j on the sensitivity of node i to node k with a bilinear term $a_{ijk} x_j x_k$.

Parameter sampling vs. estimation. In the method suggested here, a parameter sampling strategy rather than a parameter estimation strategy is applied. The idea behind it is to go beyond the "average response" criticized by Trewavas (10) and consider the distribution of the experimentally observed responses. Indeed, biological replicates differ one from another because each individual is to some extent unique, and this uniqueness can be related to the model parameters. One could argue that each biological replicate has a somewhat different parameter vector. Therefore, instead of considering an average response and estimating a vector of

optimal parameters, as is commonly done, we sample the parameter space according to a particular distribution that depends on the distribution of the experimental data. Let Ω be this m-dimensional experimental read-out distribution, where m is the number of different conditions and genotypes (i.e., the size of λ). In other words, Ω is the distribution of measured hypocotyl elongations, where each mutant and experimental condition runs along a different dimension. Because the conditions are independent, this distribution is assumed to be Gaussian with a diagonal covariance matrix. Using a Markov chain Monte Carlo method (GaA-MCMC) (11), we then sample a parameter vector θ according to

$$p(\theta) \propto p_{\Omega}[g(\theta, \lambda)].$$

In other words, θ is sampled such that the distribution of the corresponding network outcomes $g(\theta, \lambda)$ follows Ω, the experimental distribution of the hypocotyl elongation. Each point θ of the parameter space is thus (theoretically) assigned a probability, and this probability corresponds to the probability of observing $g(\theta, \lambda)$ according to Ω. The distribution $p(\theta)$ captures our uncertainty of the parameter values as we do not settle for a single parameter vector, but assign a probability to the whole parameter space. This probability distribution enables the exploitation of the information contained in the variance of the experimental data (both in terms of biological regulation and experimental uncertainties), and not only its average as done by classical parameter optimization. Having a distribution on the network parameters θ allows us to predict the effect of a new knockout mutant by solving the network equation at steady state for each of the sampled parameters and looking at the distribution of responses. The mean of the resulting response provides a prediction and its variance gives a measure of confidence in this prediction.

This approach is similar to the approximate Bayesian computation (ABC) methods often used for stochastic models in population genetics (12) and that have also been applied to model selection (13). These methods also sample the parameter space, for example, with MCMC (14), and the probabilistic (or varying) outcome of the model for each parameter θ is compared with the distribution of the observed data. This sampling is done to estimate the posterior likelihood function of θ, which can then be maximized. In contrast, in our case, each parameter θ generates a single output, and the distribution of θ in the biological samples is estimated by matching the distribution of corresponding model outcome to distribution of the observations. In this sense, it can hardly be said to be a Bayesian likelihood function and the Bayes factor (essentially a likelihood ratio) cannot be used for model selection. Instead we use leave-one-out cross-validation, as described below.

Network evaluation. To evaluate the network, we look at the accuracy of its predictions in a leave-one-out cross-validation scheme. All but one mutant data are used to sample the parameter space (as described above), and the resulting parameter distribution is then used to predict the elongation of the remaining mutant (called the test mutant). This prediction is done by estimating the mean of the distribution of elongations of the test mutant when sampling from the distribution of parameters. This procedure is applied for all mutants, providing a prediction for each mutant in normal and simulated shade conditions. The Mahalanobis distance between the predicted and the observed mean elongations are then used to quantify the accuracy of the predictions. This distance is equivalent to the absolute log z-score of the predictions according to the experimental distribution of elongations. It thus reflects how well the network can capture the essential features of the biological system. If the distance is zero, it means that all mean mutant elongations are perfectly predicted. The bigger the distance is, the poorer the predictions are (and thus the network). Because the sampling entails some randomness, we assess the reliability of the predictions and evaluation by running the evaluation procedure 10 times and looking how much they vary from one another. The final score is the average score across the 10 runs. This procedure penalizes overfitting, as can be seen from the simulation results where having both the sensitivity and production of the PIFs in the network does not produce a better score than having just one of them (Fig. 2*C* vs. Fig. S2 and Fig. S5 *B* vs. *C*).

Noise model. We consider the following simple elongation model, $y_{lgi} = b_{lg}x_{lgi}$, where y is the observed elongation, x is the auxin signal, b is the auxin sensitivity, and l, g, and i denote, respectively, the light condition, the genotype, and the seedling index. To model noise, we include a multiplicative noise ε and an additive measurement noise μ, obtaining $y_{lgi} = b_{lg}x_{lgi}\varepsilon_{lgi} + \mu_{lgi}$. This model is justified by the fact that the SD scales linearly with the average elongation (Fig. S9). We are interested in the variance of ε, which can be interpreted as the variance in the auxin signal read-out. Assuming noise independence, we have $\mathrm{var}(\varepsilon_{lg}) = [\mathrm{var}(y_{lg}) - \mathrm{var}(\mu_{lg})]/(b_{lg}x_{lg})^2$. We estimated the variance of measurement noise $\mathrm{var}(\mu_{lg})$ (assumed to be the same for all l and g) by measuring twice the same data set, whereas $b_{lg}x_{lg}$ is estimated as the average elongation for a given light condition and genotype. Assuming normal distributions for μ (centered) and ε (centered on 1), an F test can be used to assess whether $\mathrm{var}(\varepsilon_{lg})$ varies significantly between two conditions.

1. Lorrain S, Allen T, Duek PD, Whitelam GC, Fankhauser C (2008) Phytochrome-mediated inhibition of shade avoidance involves degradation of growth-promoting bHLH transcription factors. *Plant J* 53(2):312–323.
2. Tao Y, et al. (2008) Rapid synthesis of auxin via a new tryptophan-dependent pathway is required for shade avoidance in plants. *Cell* 133(1):164–176.
3. Hornitschek P, Lorrain S, Zoete V, Michielin O, Fankhauser C (2009) Inhibition of the shade avoidance response by formation of non-DNA binding bHLH heterodimers. *EMBO J* 28(24):3893–3902.
4. Hornitschek P, et al. (2012) Phytochrome interacting factors 4 and 5 control seedling growth in changing light conditions by directly controlling auxin signaling. *Plant J* 71 (5):699–711.
5. Mendoza L, Xenarios I (2006) A method for the generation of standardized qualitative dynamical systems of regulatory networks. *Theor Biol Med Model* 3:13.
6. Andersen SU, et al. (2008) Requirement of B2-type cyclin-dependent kinases for meristem integrity in Arabidopsis thaliana. *Plant Cell* 20(1):88–100.
7. Mancinelli A (1994) The physiology of phytochrome action. *Photomorphogenesis in Plants,* eds Kendrick RE, Kronenberg GHM (Springer, New York), 2nd Ed, pp 211–269.
8. Lohmiller W, Slotine J-JE (1998) On contraction analysis for non-linear systems. *Automatica* 34(6):683–696.
9. Ciliberti S, Martin OC, Wagner A (2007) Innovation and robustness in complex regulatory gene networks. *Proc Natl Acad Sci USA* 104(34):13591–13596.
10. Trewavas A (2003) Aspects of plant intelligence. *Ann Bot (Lond)* 92(1):1–20.
11. Müller CL, Sbalzarini IF (2010) Gaussian adaptation as a unifying framework for continuous black-box optimization and adaptive Monte Carlo sampling. *IEEE World Congress on Evolutionary Computation,* July 18–23, 2010, Barcelona (IEEE, Piscataway, NJ), pp 2594–2601.
12. Marin J-M, Pudlo P, Robert CP, Ryder R (2011) Approximate Bayesian computational methods. *Stat Comput* 22(6):1167–1180.
13. Toni T, Stumpf MPH (2010) Simulation-based model selection for dynamical systems in systems and population biology. *Bioinformatics* 26(1):104–110.
14. Marjoram P, Molitor J, Plagnol V, Tavare S (2003) Markov chain Monte Carlo without likelihoods. *Proc Natl Acad Sci USA* 100(26):15324–15328.

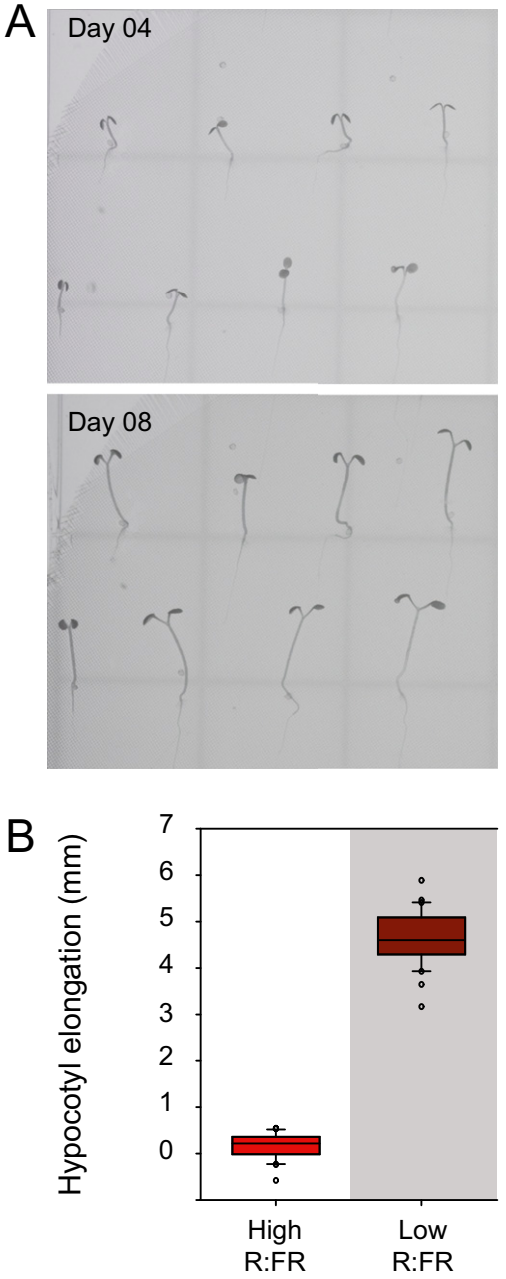

Fig. S1. Experimental setup. (*A*) Seedlings were grown on vertical plates along a nylon mesh. Pictures were taken at day 4 and day 8. (*B*) Hypocotyl elongation during the last 4 d of the experiment. Hypocotyl elongation during the treatment was measured as the difference of hypocotyl length between day 4 and day 8. $n = 25–34$, error bars = 2 SE.

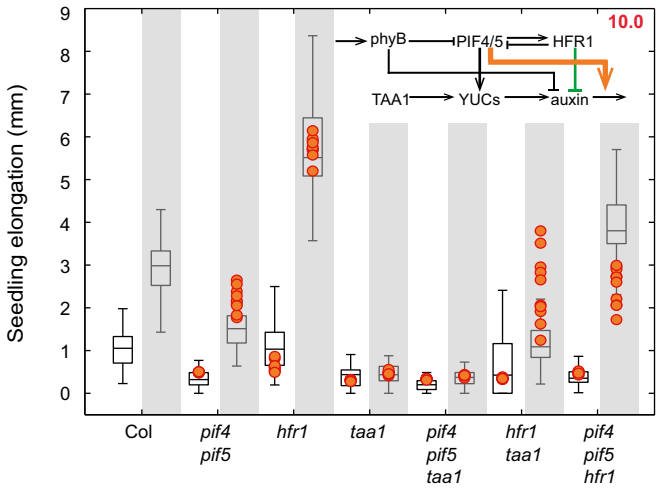

Fig. S2. Observed and predicted elongation of seedlings grown in low light intensity in normal (white background) and low R:FR (shaded background) for the network including the link between PIF and auxin production [through the YUCCA (YUC)] and auxin sensitivity.

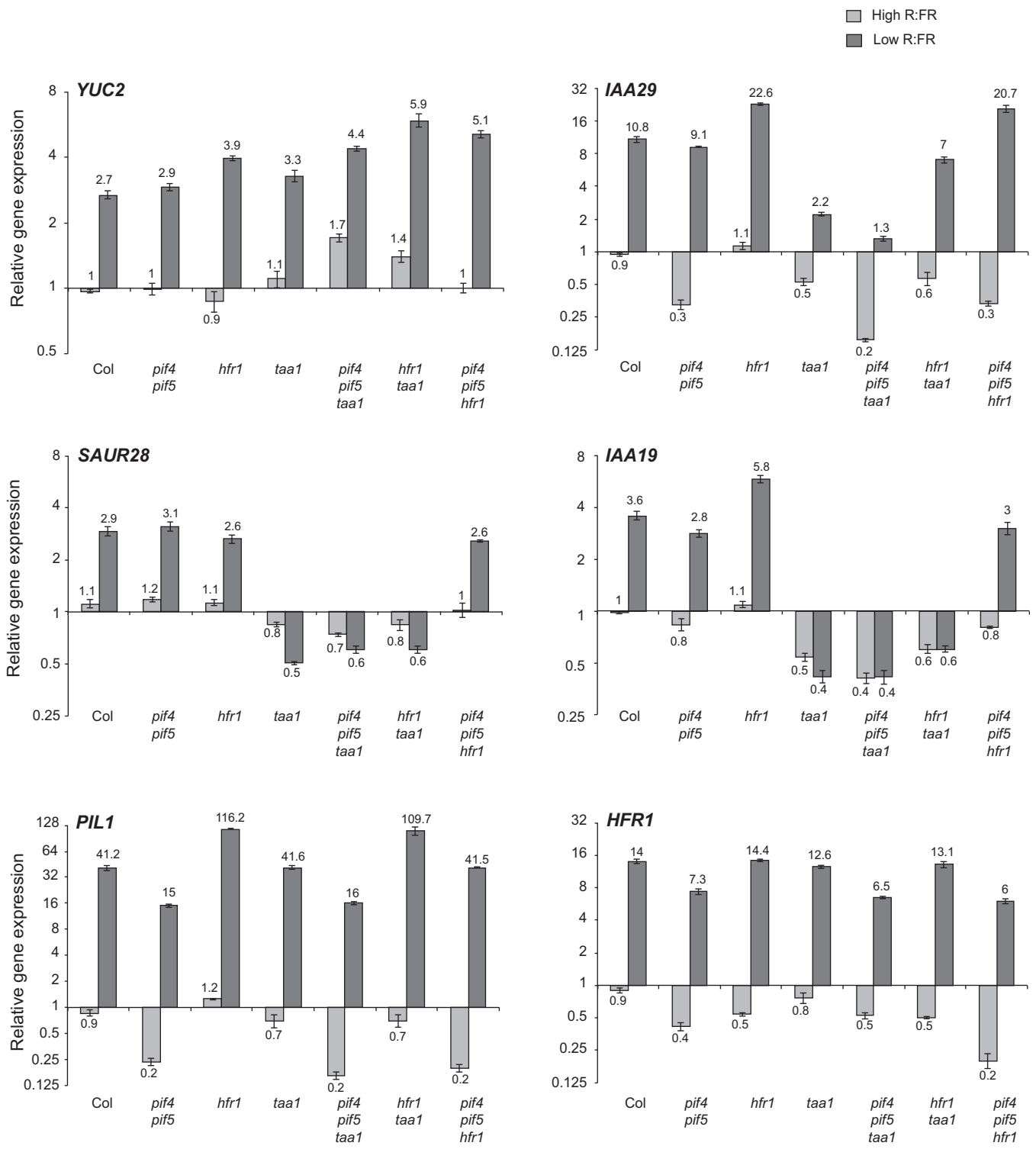

Fig. S3. Quantitative RT-PCR analysis of shade-responsive genes. The different genotypes were grown 4 d in constant high R:FR light followed by 3 d in low or high R:FR. Gene expression was normalized to *YLS8* and *UBC* and expressed relative to one WT control grown under high R:FR. Error bars represent the SEM of three biological replicates.

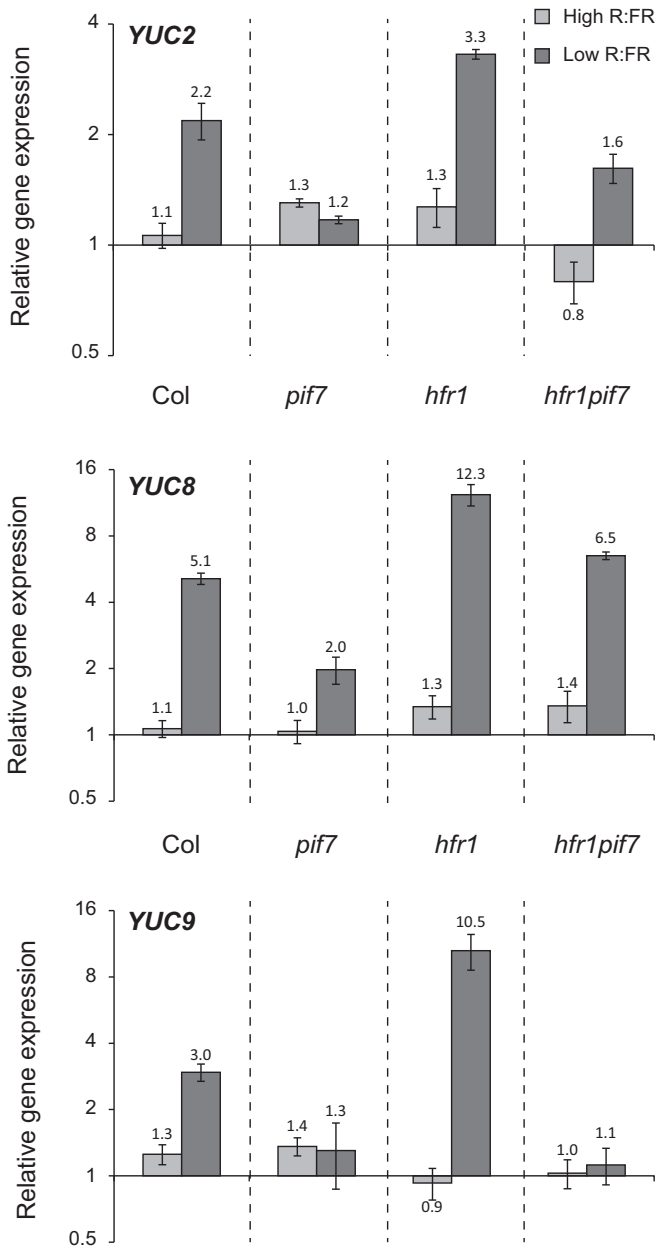

Fig. S4. Quantitative RT-PCR analysis of *YUC* genes in the *hfr1pif7* double mutant. The different genotypes were grown 4 d in constant high R:FR light followed by 3 d in low or high R:FR. Gene expression was normalized to *YLS8* and *UBC* and expressed relative to one WT control grown under high R:FR. Error bars represent the SEM of three biological replicates.

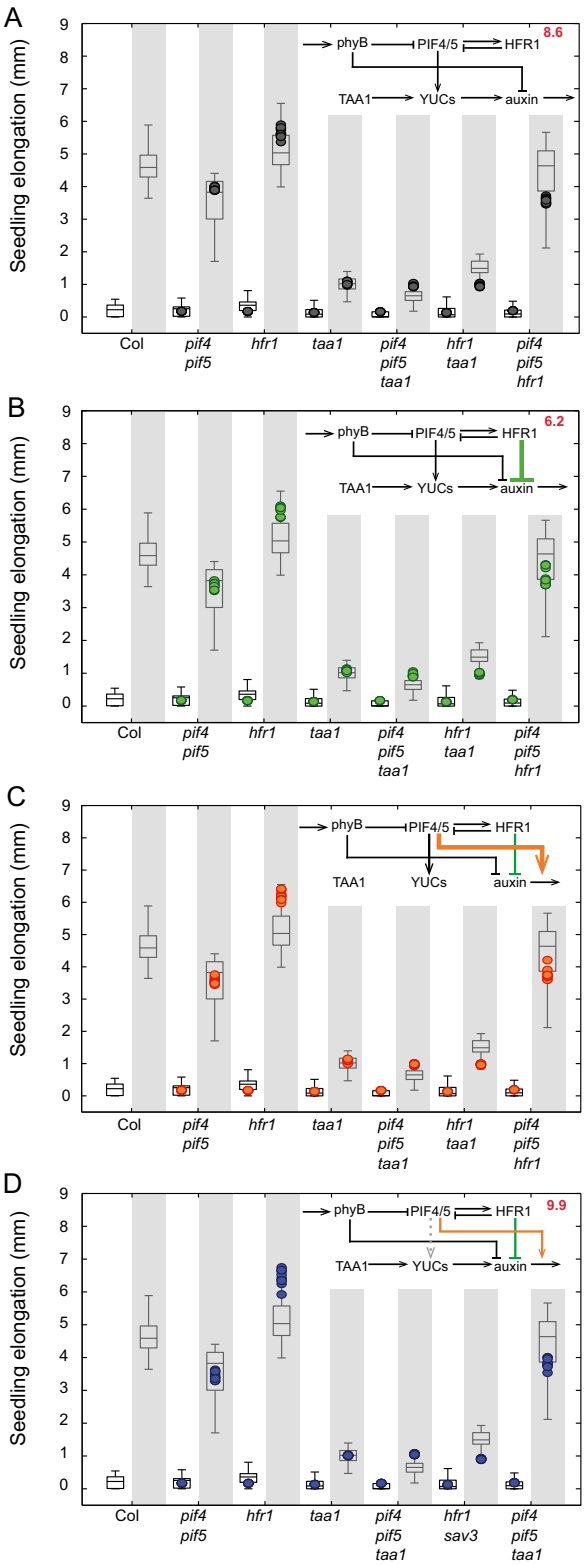

Fig. S5. (*A–D*) Observed and predicted elongation of seedlings grown in high light intensity conditions for various networks. Network B makes predictions significantly better than all other networks. Refer to the legends of Figs. 2 and 4*A* for more details.

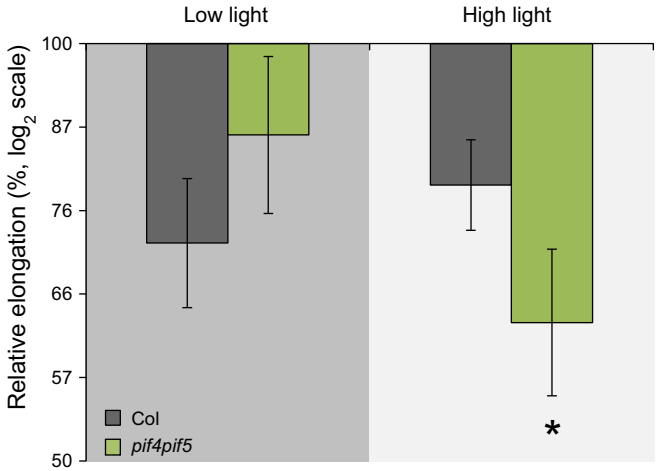

Fig. S6. Differential effect of yucasin on *pif4pif5* depending on PAR. Relative hypocotyl elongation of WT seedlings in low R:FR in presence of inhibitor of auxin synthesis (yucasin) at the concentration of 100 μM. $n > 14$, mean ± 2 SE. *Statistical difference ($P < 0.01$) using a *t* test. As previously published (1), the efficiency of yucasin to inhibit hypocotyl elongation is limited.

1. Nishimura T, et al. (2014) Yucasin is a potent inhibitor of YUCCA, a key enzyme in auxin biosynthesis. *Plant J* 77(3):352–366.

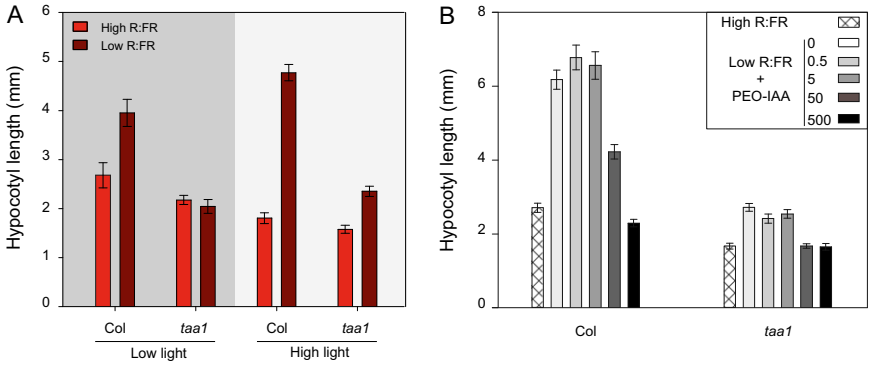

Fig. S7. Hypocotyl elongation in response to low R:FR of *taa1*. (*A*) Hypocotyl length of seedlings grown in high or low R:FR under low or high light conditions. $n = 23–30$, error bars = 2 SE. (*B*) Hypocotyl length of 8-d-old seedlings grown under high or low R:FR, high intensity in the presence of inhibitor of auxin perception (PEO-IAA). Experiments were conducted as described in Fig. 2*B*.

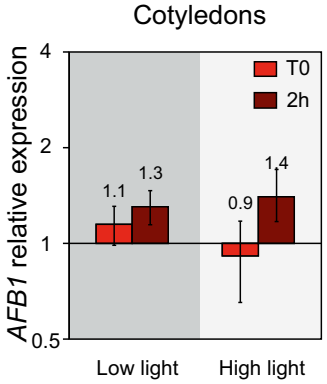

Fig. S8. *AFB1* expression is not induced in the cotyledons in response to low R:FR. Gene expression was determined by quantitative RT-PCR in cotyledons of 7-d-old WT seedlings grown in low light intensity, high R:FR (T0), or subjected for 2 h to low R:FR (2 h). Data are mean ± 2 SE ($n = 3 \times 40$ seedlings).

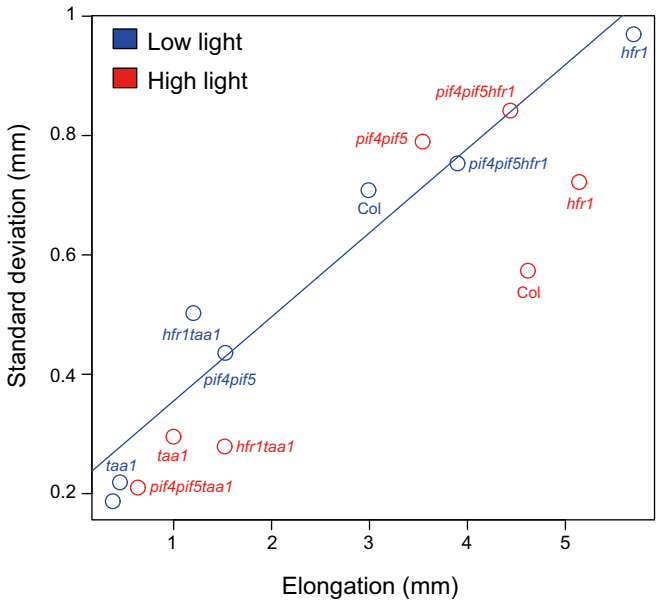

Fig. S9. Noise analysis. For most genotypes and conditions, a linear relationship is observed between mean elongation and its SD, confirming the validity of an additive and multiplicative noise model. In high light, the Col elongation displays less variability than what would be expected from its mean elongation, suggesting that the increased auxin signal intensity makes it more robust. Interestingly, this is not the case for *the pif4pif5* mutants. The regression line for low light conditions is shown in blue.

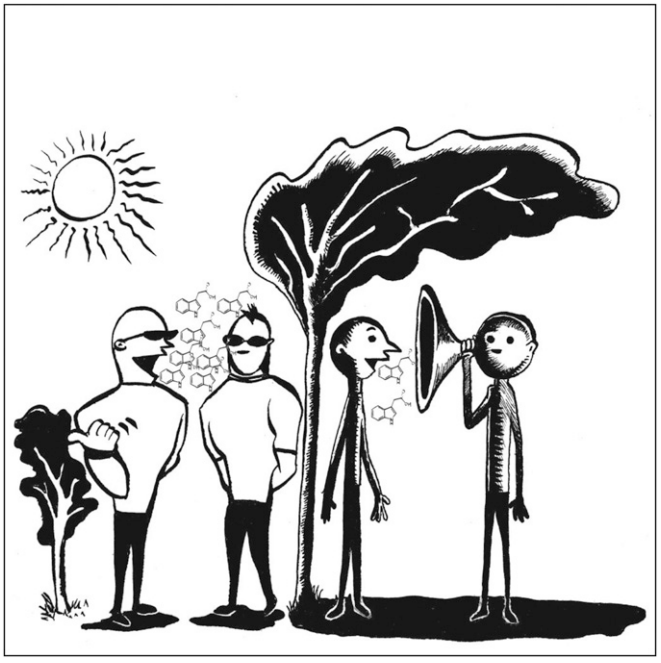

Fig. S10. Metaphorical illustration of the model. In foliar shade, a weaker signal (represented by fewer auxin molecules) is compensated by an increased sensitivity (represented by the hearing aid).